APL MATERIALS **2**, 092504 (2014)

Air stable *n*-doping of WSe_2 by silicon nitride thin films with tunable fixed charge density

Kevin Chen, Daisuke Kiriya, Mark Hettick, Mahmut Tosun, Tae-Jun Ha,[a]
Surabhi Rao Madhvapathy, Sujay Desai, Angada Sachid, and Ali Javey[b]
Electrical Engineering and Computer Sciences Department, University of California, Berkeley, California 94720, USA and Materials Sciences Division, Lawrence Berkeley National Laboratory, Berkeley, California 94720, USA

(Received 7 July 2014; accepted 21 July 2014; published online 5 August 2014)

Stable *n*-doping of WSe_2 using thin films of SiN_x deposited on the surface via plasma-enhanced chemical vapor deposition is presented. Positive fixed charge centers inside SiN_x act to dope WSe_2 thin flakes *n*-type via field-induced effect. The electron concentration in WSe_2 can be well controlled up to the degenerate limit by simply adjusting the stoichiometry of the SiN_x through deposition process parameters. For the high doping limit, the Schottky barrier width at the metal/WSe_2 junction is significantly thinned, allowing for efficient electron injection via tunneling. Using this doping scheme, we demonstrate air-stable WSe_2 n-MOSFETs with a mobility of ~70 cm^2/V s. © *2014 Author(s). All article content, except where otherwise noted, is licensed under a Creative Commons Attribution 3.0 Unported License.* [http://dx.doi.org/10.1063/1.4891824]

Two dimensional (2D) layered materials have generated much interest due to the ability to obtain atomically well-defined layers with thicknesses down to a single layer, providing a potential pathway to ultra-scaled transistors with excellent gate control.[1–4] In addition, they may enable new electronic and optoelectronic device architectures with unique functionalities.[5,6] Transition metal dichalcogenides (TMDCs) as a class of 2D materials, in particular, exhibit a wide range of electronic properties ranging from metallic to insulating,[7] with many being semiconductors with intrinsic carrier mobilities >100 cm^2/V s[8] even when scaled down to a monolayer in thickness. It should be noted that the measured mobility is high for a sub-1 nm thick semiconductor when compared to silicon or III–V semiconductors of similar thicknesses,[9] owing to the lack of surface native oxides and in principle atomically smooth surfaces which reduce surface roughness scattering of carriers. Due to this range of available materials, transistors have been made consisting of entirely 2D materials, exhibiting proof of concept for the scaling potential of layered materials.[10] However, one challenge of TMDCs is that they generally exhibit a high degree of Fermi level pinning,[11] resulting in it being very difficult to contact both the conduction band and valence band for the same material. In this regard, degenerate doping of the source/drain contacts, similar to what is often used in conventional 3D semiconductors, is the most effective route for injecting electrons or holes with low contact resistances. Furthermore, controlled n- and p-doping of TMDCs is critical for enabling various device structures. Doping of TMDCs via surface charge transfer doping has been demonstrated in the past using a variety of electron donating or withdrawing molecular species.[8,12,13] While the previous works have demonstrated the proof-of-concept viability of *n*- and *p*-doping for TMDCs, development of air-stable and scalable dopant processes is still of significant need.

In this work, we present a robust *n*-doping method for WSe_2 by depositing thin films of silicon nitride on the surface using plasma enhanced chemical vapor deposition (PECVD). PECVD nitride has been widely used for field-effect passivation of silicon solar cells[14–16] and is an air

[a]Present address: Department of Electronic Materials Engineering, Kwangwoon University, Seoul 139-701, South Korea.
[b]Author to whom correspondence should be addressed. Electronic mail: ajavey@eecs.berkeley.edu

 ©Author(s) 2014

This article is copyrighted as indicated in the article. Reuse of AIP content is subject to the terms at: http://aplmaterials.aip.org/about/rights_and_permissions Downloaded to IP: 128.32.32.134 On: Tue, 05 Aug 2014 15:57:07

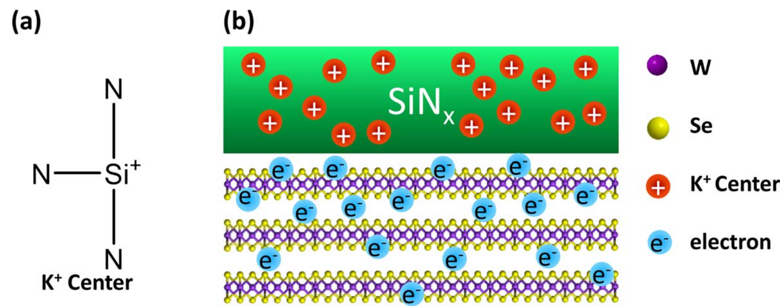

FIG. 1. (a) Diagram of the positively charged K^+ center found inside silicon nitride, originating from $Si^+ \equiv N_3$ dangling bonds. (b) Schematic of the doping mechanism of the SiN_x. The positively charged K^+ centers act as fixed charges which attract electrons inside the WSe_2, thus inverting the material.

stable[14,17] and scalable process.[18] Silicon nitride, as grown by PECVD, contains a high density of positive charge centers which originate from $^+Si \equiv N_3$ dangling bonds known as K^+ centers,[19] shown in Figure 1(a), with their density being controllable by the deposition process parameters. This characteristic is utilized in Si solar cells which induces a favorable surface band bending of Si, and thus reduces the surface recombination velocity of carriers. In fact, the field-effect induced band bending can be so severe as to cause surface inversion of *p*-body silicon.[20–22] Here, we apply the same concept to WSe_2 devices. We observe strong field-induced electron doping of WSe_2 by SiN_x coating (Figure 1(b)), with the electron sheet density being user-tunable, up to the degenerate limit by controlling the stoichiometry of the PECVD SiN_x. Notably, given the small thickness of WSe_2 (from monolayer up to ∼10 nm explored here), the entire body of WSe_2 can be inverted to *n*-type by utilizing this surface-induced field-effect doping scheme. This has enabled us to fabricate stable *n*-type WSe_2 transistors with excellent performance. More generally, the approach here presents a route towards controlling the electronic properties of TMDCs by simply depositing thin films of charged dielectrics on the surface.

Deposition of the SiN_x was done using an Oxford Plasmalab 80plus PECVD system at 13.56 MHz frequency. The deposition power, temperature, pressure, and time were kept constant for all processes at 20 W, 150 °C, 900 mTorr, and 2 min, respectively, which results in a SiN_x thickness of ∼50 nm. Silane (SiH_4, 10% in Ar) and ammonia (NH_3) were used as the process gasses and the concentrations were varied to obtain different film stoichiometries and amount of fixed charge. In this paper, the NH_3/SiH_4 ratio refers to the ratio of NH_3 to the 10% SiH_4 in Ar gas mixture. The four different NH_3/SiH_4 gas flow ratios explored were 1/10, 1/2, 1/1, and 3.3/1, corresponding to absolute NH_3/SiH_4 flow rates of 30/300, 50/100, 100/100, and 100/30 sccm, respectively.

To test the effect of different ratios of NH_3 to SiH_4 on the doping of WSe_2, back-gated WSe_2 transistors were fabricated with the device structure shown in Figure 2(a). First, WSe_2 (HQ Graphene) was mechanically exfoliated onto a heavily doped *p*-type silicon wafer (resistivity 0.001–0.005 Ω cm) with 260 nm of thermal silicon oxide, which acts as a universal back gate. To ensure that the thickness of the WSe_2 did not contribute significantly to device to device variation, the WSe_2 flakes used for devices were kept approximately constant between 5 and 10 nm in thickness via optical contrast.[23] After exfoliation, Au source (S) and drain (D) contacts were patterned and deposited using photolithography and electron-beam evaporation, respectively. Finally, SiN_x (∼50 nm in thickness) was deposited via PECVD on top of the entire sample to dope the devices.

The width normalized transfer characteristics of the WSe_2 devices at $V_{DS} = -1$ V after nitride deposition are shown in Figure 2(b) for multiple NH_3/SiH_4 process concentrations corresponding to different SiN_x stoichiometries. All devices were fabricated with a channel length of 2 μm. A representative I_{DS}–V_{GS} curve for a device before SiN_x deposition is also shown. As expected, the as-made device exhibits ambipolar transfer characteristics with slightly higher *p*-channel conductance, corresponding to close to mid-gap Schottky barriers at the source/drain metal contacts. This behavior is similar to other previous reports on WSe_2 devices with Au metal contacts.[8] Upon deposition of SiN_x, the devices exhibit *n*-type transfer characteristics with a shift in the threshold voltage

This article is copyrighted as indicated in the article. Reuse of AIP content is subject to the terms at: http://aplmaterials.aip.org/about/rights_and_permissions Downloaded to IP: 128.32.32.134 On: Tue, 05 Aug 2014 15:57:07

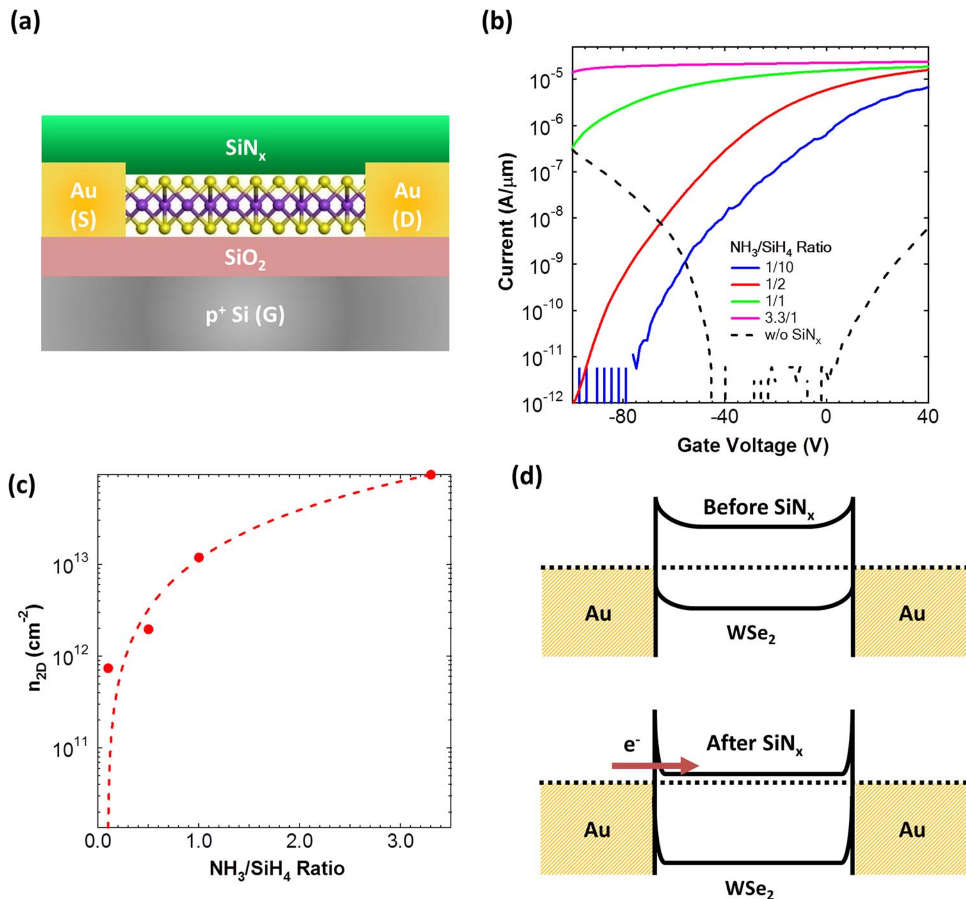

FIG. 2. (a) Schematic of the back gated WSe_2 device structure used to test the effect of NH_3/SiH_4 ratios during nitride deposition on doping. (b) Width normalized transfer characteristics of four back gated WSe_2 devices with nitride deposited using different NH_3/SiH_4 ratios. As the NH_3/SiH_4 ratio is increased, the doping level increases. To minimize the effect of device to device variation, the WSe_2 thickness was kept within the range of 5–10 nm. A representative transfer characteristic curve of a device before nitride deposition is also shown for reference. (c) Extracted two dimensional electron sheet charge densities for the four nitride deposition conditions at zero gate bias. (d) Qualitative band diagrams of the back gated devices before and after SiN_x deposition. After SiN_x deposition, the Schottky barrier width at the metal/WSe_2 contact decreases, thus enabling efficient injection of electrons by tunneling.

towards a more negative voltage. This result is indicative of electron doping of WSe_2 by SiN_x. The electron doping effect depends on the NH_3/SiH_4 ratio used during SiN_x deposition. As the NH_3/SiH_4 concentration ratio was increased, the devices become more heavily n-doped with higher n-channel conductance. Specifically, for NH_3/SiH_4 ratios of $>1/1$, WSe_2 becomes degenerately doped with minimal gate dependence in the transfer curves (Fig. 2(b)). The two dimensional electron sheet densities (n_{2D}) of the devices can be estimated from $n_{2D} = (I_{DS}L)/(q\mu WV_{DS})$,[13] where I_{DS} is the drain current at zero gate voltage, L and W are the lengths and widths of the devices, respectively, q is the electron charge, V_{DS} is the applied drain voltage, and μ is the field-effect mobility. It should be noted that this calculation does not take into account the effect of contact resistance, which may underestimate n_{2D}, especially for the lower doped devices. From Figure 2(c), it can be seen that the sheet density varies from 7.4×10^{11} to 9.5×10^{13} cm^{-1} for the explored NH_3/SiH_4 ratio. The ability to tune the electron concentration in WSe_2 by orders of magnitude by simply changing the stoichiometry of SiN_x presents a facile doping scheme. Figure 2(d) depicts a qualitative band diagram of the effect of SiN_x on WSe_2. As the devices become increasingly doped by the fixed charges in SiN_x, the Fermi level moves closer to the conduction band, shifting the threshold voltage negatively as well as reducing the width of the metal/WS_2 Schottky barrier. The thinner barrier

This article is copyrighted as indicated in the article. Reuse of AIP content is subject to the terms at: http://aplmaterials.aip.org/about/rights_and_permissions Downloaded to IP: 128.32.32.134 On: Tue, 05 Aug 2014 15:57:07

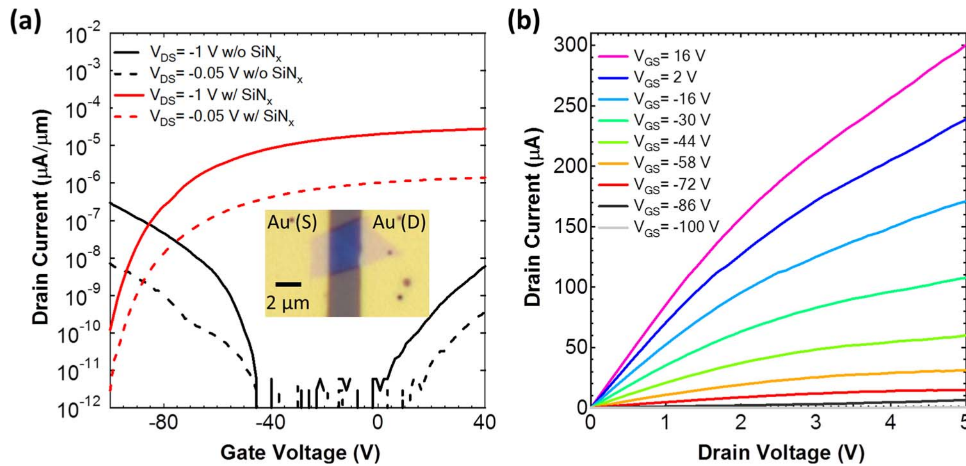

FIG. 3. (a) Transfer characteristics of a WSe_2 back-gate FET before and after SiN_x deposition at a NH_3/SiH_4 concentration ratio of 1/2. An optical image of the device is shown in the inset. (b) Output characteristics of the device post SiN_x deposition.

enables greater electron injection by tunneling through the barrier and hence forms a practical ohmic contact for electrons (Fig. 2(d)).

Figure 3(a) shows the transfer characteristics at $V_{DS} = -0.05$ and -1 V of a WSe_2 back-gated transistor two weeks after deposition of SiN_x with a NH_3/SiH_4 ratio of 1/2, which corresponds to a WSe_2 sheet electron density of 2×10^{12} cm^{-2} (Fig. 2(c)). This electron sheet density is high enough to provide a low resistance metal contact to the conduction band of WSe_2 while still allowing for gate control of the channel. The transfer characteristics of the device before doping are included for reference. An optical microscope image of the actual device is shown in the inset. This *n*-type FET exhibits a peak field-effect mobility of $\sim$70 cm^2/V s as extracted using the analytical equation $\mu = G_m L/(W V_{DS} C_{ox})$. Here, G_m is the transconductance, $C_{ox} = 1.33 \times 10^{-8}$ F/cm^2 is the calculated gate oxide capacitance for 260 nm of SiO_2, and W and L are the width and length of the channel, respectively. Figure 3(b) shows the output characteristics of the same device after nitride deposition. As can be seen, the curves are linear at low V_{DS}, indicating that the contact is near ohmic.

To understand the effect of the NH_3/SiH_4 concentration during deposition on the doping level, the fixed charge density present inside the nitride was extracted using capacitance-voltage (*C-V*) measurements. A metal insulator semiconductor (MIS) structure with an Al gate on top of SiN_x, shown in the inset of Figure 4(a), was fabricated for the *C-V* measurements. First, the SiN_x was deposited via PECVD onto a lightly doped n-type silicon wafer with resistivity between 10 and 30 Ω cm. Then, 500 $\times$ 500 μm squares of Al (150 nm in thickness) were deposited onto the nitride using a shadow mask via thermal evaporation. As can be seen in Figure 4(a), the flat band voltages of the MIS structures shift more negatively as the NH_3/SiH_4 ratio is increased for deposition. In all cases, the flat band voltage is negative with respect to the expected flat band voltage of Al and the lightly doped *n*-type wafer, given by the work function difference of $\phi_{MS} \sim -0.23$ V. This indicates the presence of positive fixed charge inside the nitride as expected. The flat band voltage, V_{FB}, can be determined as the peak of $d^2(1/C_{nitride}{}^2)/dV^2$ where $C_{nitride}$ is the accumulation capacitance of the MIS structure.[24] For 1/10, 1/2, 1/1, and 3.3/1 NH_3/SiH_4 ratios, the measured V_{FB} are approximately -4.3, -6.2, -7.4, and -9.1 V, respectively. The fixed charge density can be calculated from the shift in the V_{FB} using the equation $Q_F = C_{nitride}(\phi_{MS} - V_{FB})/\mathrm{q}$ assuming that the fixed charge is equally distributed throughout the nitride where q is the electron charge. The calculated fixed charge densities vs. the NH_3/SiH_4 gas flow ratio used during deposition is plotted in Figure 4(b). As can be seen, the fixed charge densities increase monotonically as the ratio of NH_3 to SiH_4 is increased, which results in the higher doping levels observed in these devices.

Fourier transform infrared spectroscopy (FTIR) measurements were conducted on SiN_x films deposited at different NH_3/SiH_4 concentration ratios to measure the relative amounts of Si-H bonds. Figure 4(c) shows the FTIR spectra at $\sim$2100 cm^{-1}, which corresponds to the Si–H stretching

This article is copyrighted as indicated in the article. Reuse of AIP content is subject to the terms at: http://aplmaterials.aip.org/about/rights_and_permissions Downloaded to IP: 128.32.32.134 On: Tue, 05 Aug 2014 15:57:07

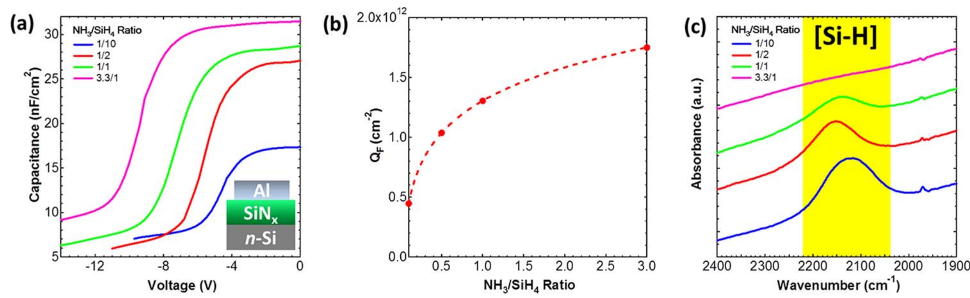

FIG. 4. (a) Capacitance-voltage (*C-V*) curves for silicon nitride films deposited at different NH_3/SiH_4 concentration ratios. The device schematic is shown in the inset. (b) Plot of the extracted fixed charge density in the silicon nitride films as a function of NH_3/SiH_4 ratio. As the ratio is increased, the fixed charge density increases. (c) Fourier transform infrared spectroscopy of the Si–H stretching mode at $\sim$2100 cm^{-1}. As the NH_3/SiH_4 ratio is increased, the Si–H bond density drops and the peak shifts to higher wavenumbers, corresponding to a more nitrogen rich nitride films and larger concentration of K centers.

mode.[25] As can be seen, the integrated Si–H peak intensity drops as the NH_3/SiH_4 ratio is increased, indicating a reduced amount of Si–H bonds. In addition, the peak position shifts from $\sim$2129 cm^{-1} at 1/10 NH_3/SiH_4 to $\sim$2190 cm^{-1} at 3.3/1 NH_3/SiH_4 which corresponds to an increase in the N_3Si–H bonding configuration component of the Si–H stretching mode[26] which has a peak position at 2220 cm^{-1}. This peak shift also indicates a stoichiometry change from silicon rich to a more nitrogen rich SiN_x.[27] The drop in integrated peak intensity and shift towards higher wavenumbers has been correlated with an increased density of dangling bond K centers.[27]

Due to the use of a plasma during the nitride deposition, it is possible that the surface of the WSe_2 can be damaged. To explore the effect of the PECVD deposition on the integrity of WSe_2, a back-gated monolayer WSe_2 transistor with Pd S/D contacts was fabricated. As the device is a single layer, any surface damage would result in drastic changes to its electronic and optoelectronic properties. An optical image of the device after doping is shown in Figure 5(a). The transfer characteristics of the monolayer before and after nitride deposition using an NH_3/SiH_4 ratio of 1/2 are plotted in Figure 5(b). Just as with the thicker WSe_2 devices, the monolayer device shows good *n*-type behavior after nitride deposition. To further explore the effect of the PECVD on the WSe_2, photoluminescence (PL) and Raman spectroscopy (HORIBA LabRAM HR800, 532 excitation wavelength) were carried out before and after nitride deposition. To ensure that no damage or measurement artifacts would result from sample heating, the laser power used was 0.8 mW. As seen in Figure 5(c), after SiN_x deposition, a redshift of 16 meV is observed in the PL peak energy in addition to a 35× decrease in the peak intensity. This observation is consistent with the previous gated PL measurements of monolayer TMDCs and can be attributed to the formation of negatively charged trions from excitons due to the increase in electron concentration.[28–30] Similarly, in Figure 5(d), a 5× decrease in the Raman intensity as well as a peak shift of 0.7 cm^{-1} of the E^1_{2g} raman peak can be attributed to a softening of the vibrational modes due to the increase in electron concentration, which has been observed in monolayer MoS_2 devices.[12,31] Overall, no unexpected change in the electronic and optoelectronic properties of the monolayer WSe_2 was observed after SiN_x deposition, indicating that the deposition process does not affect the crystalline integrity of the WSe_2.

In conclusion, we have demonstrated an air stable n-doping scheme for TMDCs using PECVD SiN_x with tunable fixed charge density arising from positively charged $^+Si{\equiv}N_3$ dangling bonds. By tuning the gas flow ratios of NH_3 and SiH_4, different densities of fixed charge within the nitride up to 1.75×10^{12} cm^{-2} are demonstrated, allowing for a controlled method to change the doping concentration via field-effect. Using this doping scheme, WSe_2 n-MOSFETs were fabricated, exhibiting a high electron mobility of $\sim$70 cm^2/V s. Similar to that of modulation doping utilized in high electron mobility transistors where the dopant atoms are away from the actual channel material, field-effect doping can enable high doping concentrations in TMDCs without causing damage to the lattice nor experiencing a drop in mobility due to ionized impurity scattering. Given the ease of processing of SiN_x and its stability as an inorganic thin film, the approach here presents a robust

This article is copyrighted as indicated in the article. Reuse of AIP content is subject to the terms at: http://aplmaterials.aip.org/about/rights_and_permissions Downloaded to IP: 128.32.32.134 On: Tue, 05 Aug 2014 15:57:07

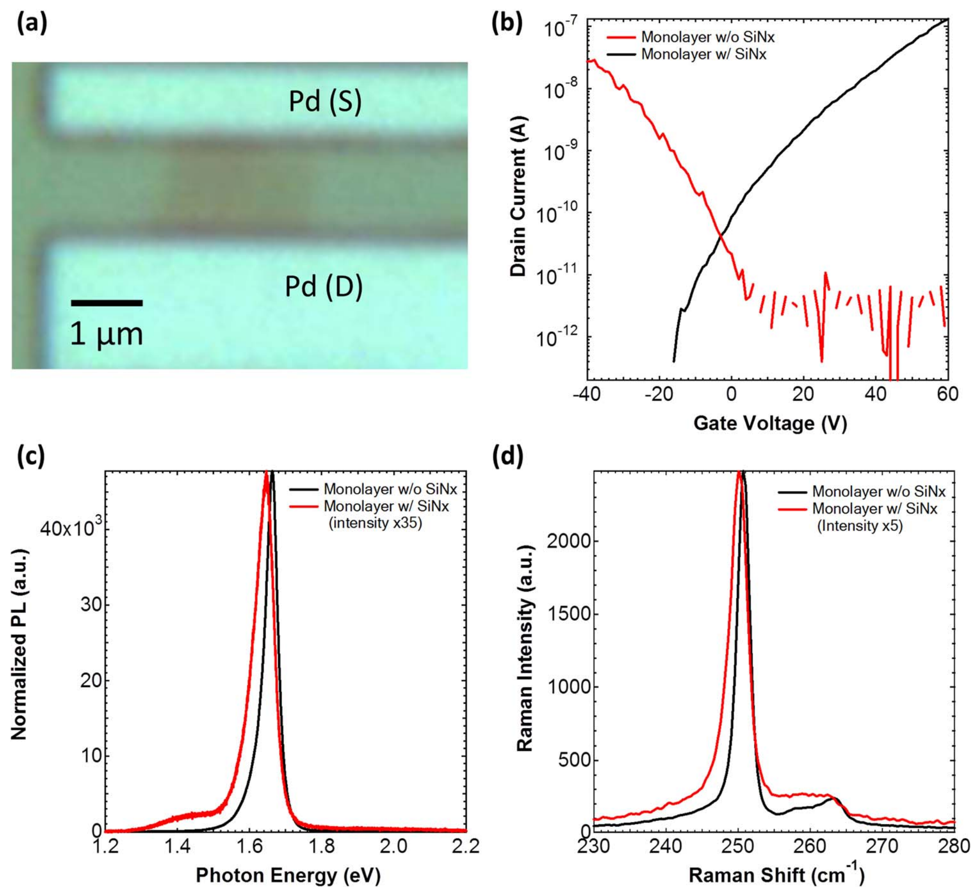

FIG. 5. (a) Optical image of a monolayer WSe_2 back-gated transistor after SiN_x deposition. (b) Transfer characteristics of the device before and after SiN_x deposition. (c) Photoluminescence and (d) Raman spectra (excitation wavelength of 532 nm) of the monolayer before and after SiN_x deposition indicating no damage to the flake occurred during nitride deposition.

route towards controlled doping of thin layers of TMDCs. In the future, the use of dielectrics with negative fixed charges can be explored as a complementary *p*-doping scheme.

Deposition of SiN_x was funded by the NSF NASCENT Center. Other material processing and characterization was funded by the Director, Office of Science, Office of Basic Energy Sciences, Material Sciences and Engineering Division, U.S. Department of Energy, under Contract No. DE-AC02-05CH11231. Device fabrication was funded by the Center for Low Energy Systems Technology (LEAST), one of six centers supported by the STARnet phase of the Focus Center Research Program (FCRP), a Semiconductor Research Corporation program sponsored by MARCO and DARPA.

[1] K. I. Bolotin, K. J. Sikes, Z. Jiang, M. Klima, G. Fudenberg, J. Hone, P. Kim, and H. L. Stormer, Solid State Commun. **146**, 351 (2008).
[2] Q. H. Wang, K. Kalantar-Zadeh, A. Kis, J. N. Coleman, and M. S. Strano, Nat. Nanotechnol. **7**, 699 (2012).
[3] B. Radisavljevic, A. Radenovic, J. Brivio, V. Giacometti, and A. Kis, Nat. Nanotechnol. **6**, 147 (2011).
[4] H. Liu, A. T. Neal, and P. D. Ye, ACS Nano **6**, 8563 (2012).
[5] B. W. H. Baugher, H. O. H. Churchill, Y. Yang, and P. Jarillo-Herrero, Nat. Nanotechnol. **9**, 262 (2014).
[6] J. S. Ross, P. Klement, A. M. Jones, N. J. Ghimire, J. Yan, D. G. Mandrus, T. Taniguchi, K. Watanabe, K. Kitamura, W. Yao, D. H. Cobden, and X. Xu, Nat. Nanotechnol. **9**, 268 (2014).
[7] M. Chhowalla, H. S. Shin, G. Eda, L.-J. Li, K. P. Loh, and H. Zhang, Nat. Chem. **5**, 263 (2013).
[8] H. Fang, M. Tosun, G. Seol, T. C. Chang, K. Takei, J. Guo, and A. Javey, Nano Lett. **13**, 1991 (2013).
[9] M. Schmidt, M. C. Lemme, H. D. B. Gottlob, F. Driussi, L. Selmi, and H. Kurz, Solid-State Electron. **53**, 1246 (2009).
[10] T. Roy, M. Tosun, J. S. Kang, A. B. Sachid, S. B. Desai, M. Hettick, C. C. Hu, and A. Javey, ACS Nano **8**, 6259 (2014).
[11] S. Das, H.-Y. Chen, A. V. Penumatcha, and J. Appenzeller, Nano Lett. **13**, 100 (2013).
[12] D. Kiriya, M. Tosun, P. Zhao, J. S. Kang, and A. Javey, J. Am. Chem. Soc. **136**, 7853 (2014).
[13] H. Fang, S. Chuang, T. C. Chang, K. Takei, T. Takahashi, and A. Javey, Nano Lett. **12**, 3788 (2012).

This article is copyrighted as indicated in the article. Reuse of AIP content is subject to the terms at: http://aplmaterials.aip.org/about/rights_and_permissions Downloaded to IP: 128.32.32.134 On: Tue, 05 Aug 2014 15:57:07

[14] A. G. Aberle, Sol. Energy Mater. Sol. Cells **65**, 239 (2001).
[15] T. Lauinger, J. Schmidt, A. G. Aberle, and R. Hezel, Appl. Phys. Lett. **68**, 1232 (1996).
[16] V. Sharma, C. Tracy, D. Schroder, S. Herasimenka, W. Dauksher, and S. Bowden, Appl. Phys. Lett. **104**, 053503 (2014).
[17] A. G. Aberle and R. Hezel, Prog. Photovolt. Res. Appl. **5**, 29 (1997).
[18] J. D. Moschner, J. Henze, J. Schmidt, and R. Hezel, Prog. Photovolt. Res. Appl. **12**, 21 (2004).
[19] J. Robertson, Philos. Mag. B **69**, 307 (1994).
[20] S. Dauwe, L. Mittelstädt, A. Metz, and R. Hezel, Prog. Photovolt. Res. Appl. **10**, 271 (2002).
[21] R. Hezel and K. Jaeger, J. Electrochem. Soc. **136**, 518 (1989).
[22] R. Schorner, R. Hezel, and R. Hezel, IEEE Trans. Electron Dev. **28**, 1466 (1981).
[23] M. M. Benameur, B. Radisavljevic, J. S. Héron, S. Sahoo, H. Berger, and A. Kis, Nanotechnology **22**, 125706 (2011).
[24] D. K. Schroder, *Semiconductor Material and Device Characterization* (John Wiley and Sons, 2006).
[25] G. Scardera, T. Puzzer, G. Conibeer, and M. A. Green, J. Appl. Phys. **104**, 104310 (2008).
[26] E. Bustarret, M. Bensouda, M. C. Habrard, J. C. Bruyère, S. Poulin, and S. C. Gujrathi, Phys. Rev. B **38**, 8171 (1988).
[27] H. Mäckel and R. Lüdemann, J. Appl. Phys. **92**, 2602 (2002).
[28] K. F. Mak, K. He, C. Lee, G. H. Lee, J. Hone, T. F. Heinz, and J. Shan, Nat. Mater. **12**, 207 (2013).
[29] S. Mouri, Y. Miyauchi, and K. Matsuda, Nano Lett. **13**, 5944 (2013).
[30] A. M. Jones, H. Yu, N. J. Ghimire, S. Wu, G. Aivazian, J. S. Ross, B. Zhao, J. Yan, D. G. Mandrus, D. Xiao, W. Yao, and X. Xu, Nat. Nanotechnol. **8**, 634 (2013).
[31] B. Chakraborty, A. Bera, D. V. S. Muthu, S. Bhowmick, U. V. Waghmare, and A. K. Sood, Phys. Rev. B **85**, 161403 (2012).

This article is copyrighted as indicated in the article. Reuse of AIP content is subject to the terms at: http://aplmaterials.aip.org/about/rights_and_permissions Downloaded to IP: 128.32.32.134 On: Tue, 05 Aug 2014 15:57:07